Tech Science Press

# Prediction of Outdoor Noise Propagation Induced By Single-Phase Power Transformers

**Xueyun Ruan[1,2], Wei Huang[1], Linke Zhang[3] and Yan Gao[2,*]**

[1]School of Mechanical Engineering, Anhui University of Science and Technology, Anhui Huainan, 232000, China.
[2]Key Laboratory of Noise and Vibration Research, Institute of Acoustics, Chinese Academy of Sciences, Beijing, 100190, China.
[3]School of Energy and Power Engineering, Wuhan University of Technology, Hubei Wuhan, 430063, China.
[*]Corresponding Author: Yan Gao. Email: gaoyan@mail.ioa.ac.cn.

**Abstract:** Outdoor power transformers are one of the most pervasive noise sources in power transmission and distribution systems. Accurate prediction of outdoor noise propagation plays a dominant role for the evaluation and control of noise relevant to the transformer stations. In this paper surface vibration tests are carried out on a scale model of a single-phase transformer tank wall at different excitation frequencies. The phase and amplitude of test data are found to be randomly distributed when the excitation frequency exceeds the seventh mode frequency, which allows the single-phase power transformer to be simplified as incoherent point sources. An outdoor-coherent model is subsequently developed and incorporated with the image source method to investigate noise propagation from single-phase power transformers, due to the occurrence of multiple reflections and diffractions in the propagation path of each point source. The proposed model is used to calculate the sound field of the power transformer group by exploiting the additional phase information. In comparison with the ISO9613 model and the boundary element method, it is found that the proposed coherent image source method leads to more accurate prediction results, and hence better performance for the prediction of the outdoor noise induced by single-phase power transformers.

**Keywords:** Single-phase transformer; surface vibration; scale model; noise prediction; coherent image source method

## 1 Introduction

With growing electricity demands in China, large power transformers are now being increasingly installed in urban areas. The low-frequency noise generated by power transformers has been a major issue due to the social and environmental consequences [1]. Significant research work has been devoted to studying the noise and vibration induced by transformer stations. Much of earlier research has involved the theoretical and experimental investigations into the generation mechanisms and acoustical characteristics of noise sources, along with some technological and environmental protection standards formulated in different countries [2,3].

Gordon [4] proposed a method for predicting the audible noise emissions from large outdoor power transformers. In his study, the power transformer was simplified as a point source, and the sound field was calculated according to the radiation law of point source. In later work by Usry et al. [5] and Ming et al. [6], the surface normal acceleration data were collected from transformer tanks, which were then used to predict the sound pressure according to the Helmholtz formula of integration. They showed that for the transformer dimension being significantly smaller compared with the distance between the measurement point and the transformer, the transformer can be modelled effectively as a point source. However there are still a number of gaps in their work. The coherent interference due to tank walls, adjacent transformers, and surrounding buildings was not taken into account in the model. Moreover, it is often difficult to acquire the surface

acceleration of power transformers on site, which limits the method in practical applications.

More recently the power transformer has been modelled as multiple point sources to overcome the concerns in the development of the outdoor-coherent acoustic model. Jin and Pan [7] made noise and vibration measurements of a 110 kV three-phase power transformer. They found that the noise and vibration spectra were both concentrated in the frequency range of 100 Hz~500 Hz, with the corresponding amplitudes exhibiting similar performance. They further set up the relationship between the noise and vibration generated by the power transformer. Similar behaviour was found by Bai et al. [8] in their study of noise and vibration from a 160 KVA dry-type transformer under DC bias magnetic conditions.

In this study, a coherent image source model is proposed to predict outdoor noise induced by power transformers. Surface vibration measurements are first made on the scale model of a power transformer tank wall. Special considerations in the model include wave reflections and diffractions with respect to practical configurations of outdoor power transformers. Numerical calculations of noise radiation from three power transformers with phase differences are conducted to evaluate the performance of the proposed model in comparison with the ISO9613 model and the boundary element method (BEM).

## 2 Outdoor Noise Generated by Power Transformers

Two main sources of noise from a power transformer include the body of the power transformer and the cooling system. Noise from the power transformer body is mainly caused by magnetostriction of the iron core, i.e., the phenomenon of the slight variation in the length of the silicon steel sheet of the iron core in the alternating magnetic field. Due to the nonlinearity in the magnetostriction and the different lengths of flux paths along the internal and external frames of the iron core, the iron core vibration differs from the winding vibration. Correspondingly, noise spectra generated by the body of the power transformer includes both the fundamental and high-order harmonic frequency contents [9,10].

Fig. 1 plots the noise spectrum measured at a distance of 3 m from a 110 kV transformer. It can be observed that the noise spectrum of the power transformer is concentrated in the frequency range from 100 Hz to 400 Hz, in particular at 100 Hz, 200 Hz, and 300 Hz. The measured noise spectrum is dominated by the low- and middle-frequency contents. Specifically, the low-frequency noise has received increasingly attention, since it has detrimental impacts on the living and working environments due to its long wavelengths that can propagate at long distances with small attenuation, along with the property of strong diffraction.

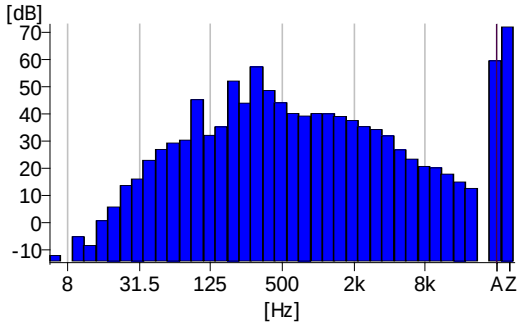


**Figure 1:** Noise spectrum of the 110 kV power transformer

## 3 Model of the Outdoor-Coherent Image Source

In general when a receiver is located sufficiently far from the noise source, it can be modelled as a point source. However, the simplified analysis is not applicable to power transformers due to their large sizes and the occurrence of reflections and diffractions caused by firewalls. In this circumstance instead of a single point source, the phases and amplitudes of different point sources need be accounted for in the

analysis. In previous research on noise prediction, the equivalent method was generally adopted to calculate the sound pressure amplitude of the simplified sound source; however, the phase and amplitude information is not considered in the energy method. This study explores the coherent sound field generated by multiple reflections of sound rays, with special considerations given to phase pertaining to the sound pressure of a point source. Measurements of vibration responses on the surface of a power transformer tank are initially made to obtain the phase and amplitude information about a point source.

### *3.1 Vibration Test on the Scale Model*

For safety reasons and limited testing condition, setting up a large amount of measuring points for vibration test of the transformer on site become extremely difficult. Thus, based on the similarity theory, a scale model of the power transformer tank wall is designed and studied in this section. Measurements of the vibration mode are made on the surface points of the scale model to lead to the phase and amplitude information of the source.

#### *3.1.1 Scale Model*

The design of the scale model follows the similarity principles, including geometric and physical similarities. In this special case, the size, wavelength, frequency, and sound field relationships are set up between the scale model and the prototype. When the geometric similarity ratio between the scale model and the prototype is 1:n, one may get the relationships as follows [11]:

$$\begin{cases} L_m = L / n \\ \lambda_m = \lambda / n \\ f_m = nf \end{cases} \tag{1}$$

where $L_m$, $\lambda_m$, and $f_m$ are the dimension, wavelength, and frequency of the scale model respectively; $L$, $\lambda$, and $f$ are the dimension, wavelength, and frequency of the prototype respectively.

In the test, the scale model was set as 1:10 with reference to the largest tank wall of the main radiation surface of the transformer. Besides, the scale model only consisted of the vertical corrugated structure composed of Q235. The geometric dimensions of the vertical reinforced tank wall model were 900 mm (length) × 450 mm (width) × 0.5 mm (thickness). Eight reinforced bars were distributed evenly on the tank wall and the metal pressing plates. Furthermore, to support the structure, the four sides were connected with the heavy and rigid test box. The geometric structure is shown in Fig. 2.

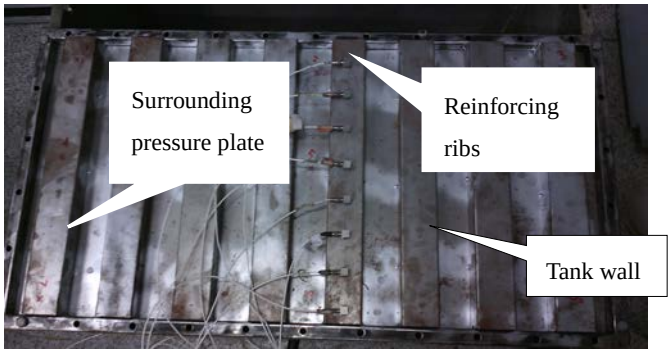


**Figure 2:** Photograph showing the scale model of the transformer tank wall

As discussed in the preceding section, the dominant frequencies of the power transformer lie between 100 Hz and 400 Hz. For the scale ratio of n=10, the phase and amplitude of vibration distribution at different measuring points on the surface are now investigated under sine excitations frequencies from

1000 Hz to 4000 Hz, including 100 Hz, 200 Hz, 400 Hz, 600 Hz, 800 Hz, 1000 Hz, 2000 Hz, 3000 Hz, and 4000 Hz. In the experiments, the exciter was placed directly below the lower side of the scale model. To facilitate the observation of the vibration distribution on the tank wall surface, the grid consisted of 120 measurement locations with a spacing of 0.05 m on the model surface, as shown in Fig. 3. In addition, the phase and amplitude of vibration response were obtained relative to a fixed reference point at the center of model. The experimental set-up for surface vibration measurements is shown in Fig. 4.

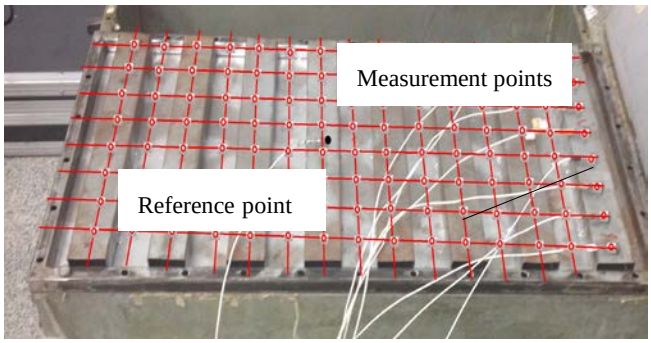


**Figure 3:** Grid of measurement points on the model surface of the power transformer

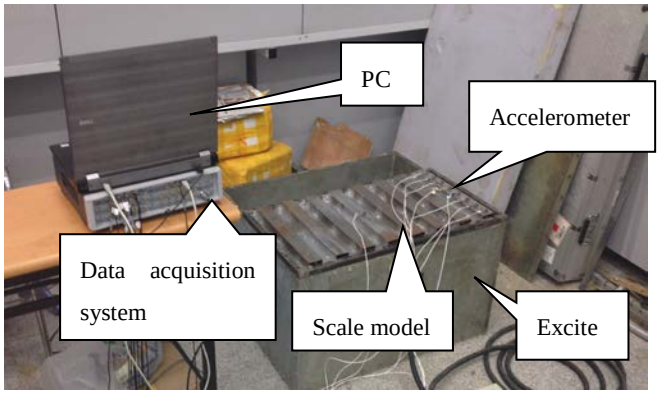


**Figure 4:** Experimental set-up for surface vibration measurements on the scale model of the power transformer

*3.1.2 Tests and Discussions*

Modal testing was conducted on the scale model before the vibration mode test at different measuring points. Tab. 1 lists the eight-order modal frequencies obtained by using the LMS Test.Lab software.

**Table 1:** First eight order modal frequencies of the scale model of the power transformer

| Order | 1 | 2 | 3 | 4 | 5 | 6 | 7 | 8 |
|---|---|---|---|---|---|---|---|---|
| Frequency (Hz) | 76.53 | 113.89 | 178.62 | 216.89 | 241.36 | 351.52 | 388.38 | 413.34 |

As shown in Tab. 1, the first eight orders of the modal frequency vary from 76.53 Hz to 413.34 Hz. According to the similarity principle of the scale model given by Eq. (1), the corresponding first eight orders of the actual transformer frequency are 7.65 Hz~41.33 Hz, being smaller than the dominant noise frequencies (100 Hz~400 Hz). Several excitation frequencies were used in the vibration test of the model surface, of which 100 Hz, 200 Hz, 400 Hz, and 1000 Hz were chosen in the plots of the 3D phase grid

distributions of the model surface as shown in Figs. 5 (a)-(d).

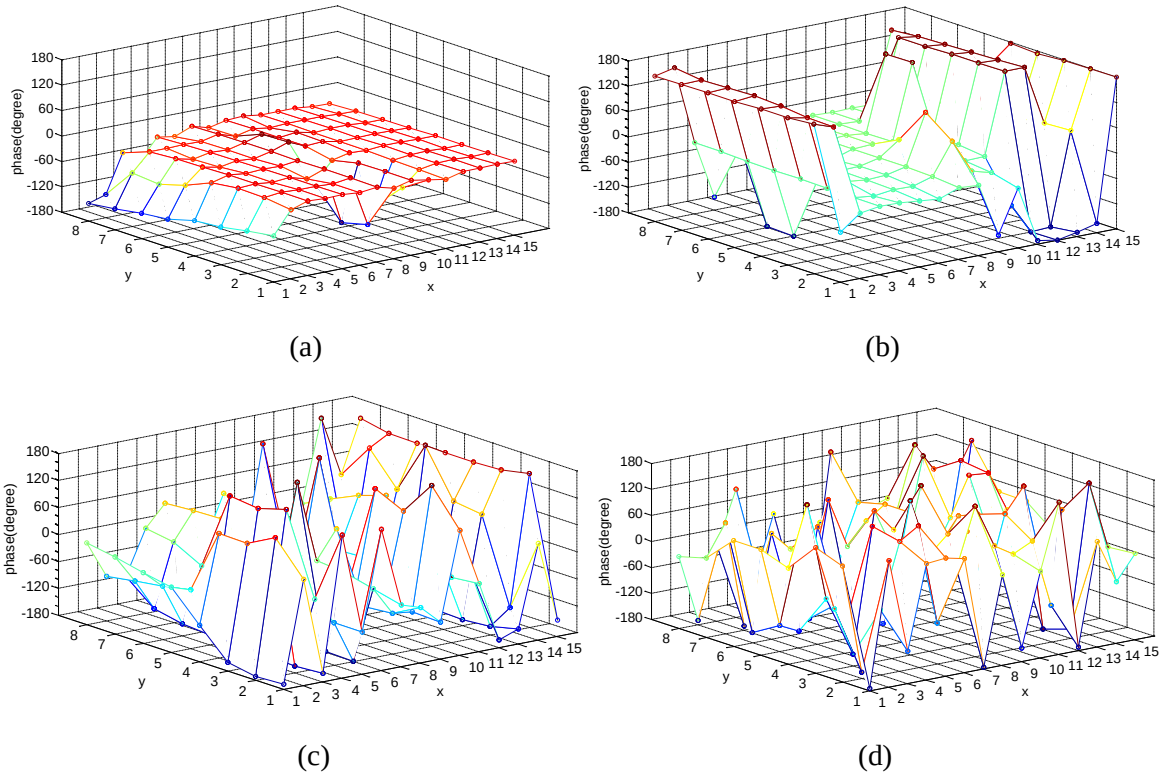


**Figure 5:** 3D phase distribution of the measurement points on the model surface: (a) 100 Hz; (b) 200 Hz; (c) 400 Hz; (d) 1000 Hz

As shown in the figures, the phases that account for 75% of the total measuring points, are mainly concentrated between -20° and 20° at the excitation frequency of 100 Hz. At 200 Hz, 51% of the total measuring points with the phases lie in -20°~20°. At 400 Hz, this figure drops to 15%, suggesting that the phase distribution become random. Indeed, at 1000 Hz, the phase at different measuring points becomes even more randomly distributed, with only 10% of the total measuring points in -20°~20° that is almost equal to the phase range of the total phase (40/360). This indicates that the measuring points in the phase range between -180° and 180° have the same probability as those between -20° and 20°. It is demonstrated that the phase range of the scale model becomes larger with the phases exhibiting random distribution with increasing excitation frequency.

Figs. 6(a-c) plot the 3D amplitude distribution of the measurement points on the model surface at the excitation frequencies of 100 Hz, 200 Hz and 400 Hz respectively. It is observed that for the lowest excitation frequency, the region with strong vibrations is mainly concentrated at the center of the model. With the increase of the excitation frequency, the stochastic behaviour of the amplitude becomes more obvious. This is mostly likely due to the complicated structure of the transformer surface where the reinforced bars have great influences on the measuring points at different locations. This is consistent with the conclusions drawn on the amplitude measurements of the cross-power spectral densities of a power transformer [6].

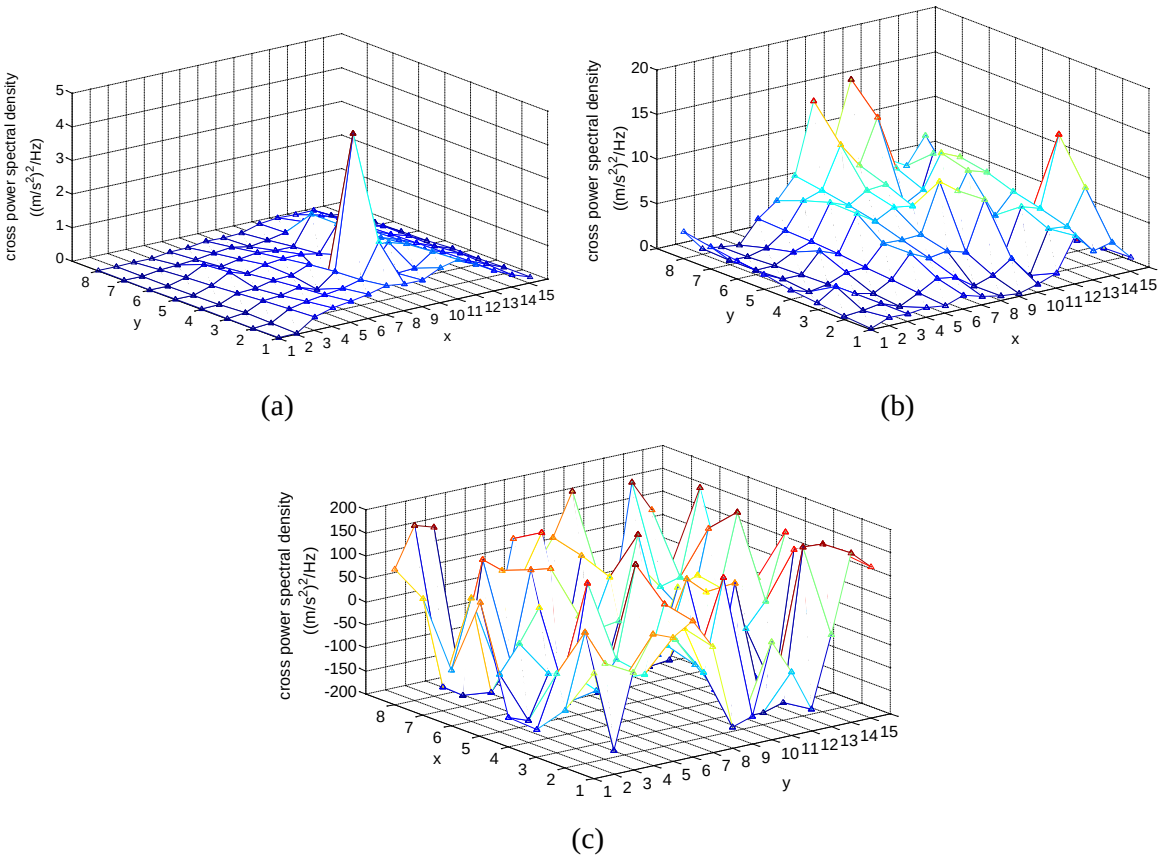


**Figure 6:** 3D amplitude distribution of the measurement points on the model surface: (a) 100 Hz; (b) 200 Hz; (c) 400 Hz

In summary, based on the theory of the scale model, measurements of the phase and amplitude information have shown the complicated surface vibration of the power transformer due to its structural features. Besides, the rigid plate structure may exhibit some high-frequency characteristics at higher excitation frequencies, which possibly results in many local modes. In this study, however, the scale model is a simple and large metal plate structure, and thus the upper limit of the dominant frequency is low. As a result, the high-frequency local modes can be neglected. For instance, in the dominant frequency range, the stochastic vibration behaviour of the scale model surface becomes more obvious as the frequency increases. For the vibration frequency of the actual transformer of 40 Hz (i.e., higher than the seventh-order frequency of 388.38/10 Hz), the stochastic behaviour of the phase and amplitude at the scattered measuring points becomes prominent, being unlikely linked to the location of the excitation point. On the one hand, for the dominant frequencies (100 Hz~400 Hz) of the noise from a power transformer, the phase and amplitude information of the power transformer surface should exhibit random distribution in the abovementioned frequency range. According to the interference theory of the sound field, interferences do not occur in the superposition of sound wave filed with a random phase. This suggests that the energy method is effective for the superposition of sound waves. In this circumstance, the single-phase transformer can be divided into equivalent point sources by the energy method without considering the phase effects.

### *3.2 Prediction Model*

Equivalent point sources on the power transformer surface, are superposed in the energy method during scale model testing. However, given the simplified point source, the multi-reflected sound waves of different point sources can interfere to result in the coherent sound field during wave radiation. It is noted that most outdoor power transformers are placed between two firewalls, and thus a resultant coherent sound field should be consider in the noise prediction. Currently available outdoor noise prediction algorithms do not require the phase information, indicating that the coherent sound field cannot be calculated. To overcome this, here a coherent image source model of the power transformer is proposed. The model is mainly used to calculate the externally coherent sound field excited by sound sources in a half-open space. Schematic diagram of the image sources is demonstrated in Fig. 7. Referring to the Fig. 7, Surfaces 1 and 2 represent the two sides of a firewall; W is the distance between two surfaces and H is the height of each surface; $R$, $E_1R$ and $E_2R$ are the receivers and diffraction points above the left and right surfaces; and $\beta_i$ (I = 1, 2, 3) represent the normalised admittances of Surfaces 1 and 2, and the ground surface.

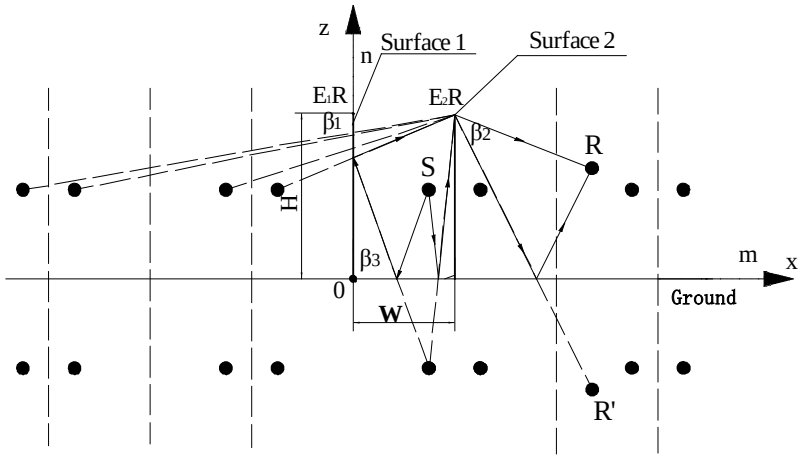


**Figure 7:** Schematic diagram of the image sources

According to the generation principle of the image source, the left-side image source ( $m \le 0$ ) starts to work when the receiver is at the right-outside part in the half-open space. Under this circumstance, the sound ray is reflected several times between two barriers and arrives at receiver R through diffraction by E2R. In contrast, the sound ray arrives at R through diffraction by E1R when the receiver is at the left-outside part in the half-open space. Here the half-open space is in an infinitely large rigid plane. Hence, the sound ray diffracted at E2R (I = 1, 2) arrives at R after it is reflected by the ground. The image receiver, $R'$, is also shown in the Fig. 7.

The entire sound field in the half-open space is determined by the overall contributions of the sound source and all image sources. Image sources are formed by the continuous reflections of the sound source by different planes. It is noted that infinite reflections generate infinite image sources. Therefore, the total sound pressure at R can be obtained as follows:

$$P = \frac{A}{4\pi} \sum_{m=-\infty}^{\infty} \sum_{n=-1}^{0} \sum_{i=1}^{2} \sum_{j=1}^{3} \left( \prod_{m} Q_1(m) \prod_{n} Q_2(m) \right) \left[ D(IS_{mn}, R | E_{ij}) + Q_{E_{ij}} D(IS_{mn}, R' | E_{ij}) \right] \left( e^{ikd_{E_{ij}IS_{mn}}} / d_{E_{ij}IS_{mn}} \right) \quad (2)$$

where A denotes the source strength coefficient of the point source; k denotes the wavenumber of the sound source; $m \in (-\infty, \infty)$ and $n \in [-1, 0]$ represents the positional parameters of the image source along x-axis and z-axis; $IS_{mn}$ is the excitation source (hereafter referred as “image source”); $IS_{00}$ is the sound

source; $i \in [1,2]$ represents surfaces 1 or 2; $j \in [1,3]$ expresses the three diffraction sides of a surface (finitely long barrier); $d_{E_{ij}IS_{mn}}$ is the distance between $IS_{mn}$ and the diffraction side $E_{ij}$; $Q_{IS_{mn}}$ is the combined complex wave reflection coefficient used to calculate the total sound reflection coefficient of all reflection surfaces corresponding to the sound waves that penetrate $IS_{mn}$ to R; $Q_{E_{ij}}$ is the reflection coefficient when the sound ray arrives at the ground after diffraction by $E_{ij}$; $d_{E_{ij}IS_{mn}}$ is the distance between $IS_{mn}$ and the diffraction side of the surface $E_{ij}R$; $D(IS_{mn}, R|E_{ij})$ and $D(IS_{mn}, R'|E_{ij})$ are the single-diffraction coefficients of the image source from $E_{ij}$ to R and from $E_i$ to $R'$, respectively (the calculation formula of the single diffraction coefficient is discussed in detail in [12]); and $Q_1(m)$ and $Q_2(n)$ are the complex sound wave coefficients of the surfaces and the ground penetrated by the sound waves.

In terms of the single-reflection coefficient of the reflection surface $Q_i$, Lemire and Nicolas [13] suggested that $Q_i$ is calculated by approximating the solution of the spherical wave reflection field on an infinitely large surface as follows [14]

$$Q_i = R_{pi} + (1 - R_{pi})F(w) \tag{3}$$

where $R_{pi}$ is the plane wave reflection coefficient of the reflection surface i, and given by

$$R_{pi} = \frac{\cos\theta_{mn} - \beta_i}{\cos\theta_{mn} + \beta_i}, i = 1,2,3 \tag{4}$$

where $\theta_{mn}$ is the angle of the normal incidence of the sound wave transmission path from $IS_{mn}$ to R on the reflection surface and $\beta_i$ is the normal specific sonar on surface i.

In Eq. (3), $F(w)$ is the loss coefficient of the interface, and is obtained by [15-17]

$$F(w) = 1 + i\sqrt{\pi}we^{-w^2}erfc(-iw) \tag{5}$$

where $erfc$ is the complementary error function; w is the numerical distance parameter related to the order number of image source (m, n), the incidence angle ($\theta_{mn}$) and the corresponding boundaries by

$$w = \sqrt{kd_{E_{ij}IS_{mn}}}(1+j)(\cos\theta_{mn} + \beta_i)/2 \tag{6}$$

It should be pointed out that the proposed coherent image source model in the half-open space include the phase information of sound sources during wave reflections or diffractions. It can thus conduct the vector superposition to calculate the outdoor-coherent sound field.

## 4 Predictions *vs.* Measurements

The formula used to predict the sound field excited by a point source in a half-open space is presented in the previous section. In this section the power transformer group is studied as shown in Fig. 8. To predict the outdoor noise radiation of the power transformer group, the single-transformer surface is first divided into several units. Each unit is equivalent to a point source. In terms of the random distribution characteristics of phases and amplitudes of unit-point sources, different point sources of the same power transformer are seen as incoherent sound sources. The source strength of an equivalent point source is calculated according to the total energy of the sound power levels (SPLs) divided by the number of point sources for an individual power transformer. Because of the phase difference of 120° in the power transformer group (composed of phases A, B and C), there is coherent interference between the sound sources of different transformers.

**Figure 8:** Power transformer group layout

### *4.1 Calculation Model*

The outdoor noise of the power transformer group is discussed using the proposed coherent image source model. In the case discussed in this paper, the model is composed of three transformers (phases A, B and C) which are distributed at certain intervals. The reflection surface consisted of four parallel firewalls and a rigid ground surface. All three transformers had the same dimensions: 4.5 m (height) × 4.0 m (length) × 9.0 m (width). The height of the firewall was 6.8 m and the length was 15 m. The distance between firewalls was 7.5 m. The firewalls and ground of the power transformer had rigid reflection surfaces, and the phase difference of the total sound sources between two adjacent transformers was 120°. Due to the regional symmetry of the transformer model, the grid size in the sound field was set to 100 m × 100 m. The grid interval dimension was 2 m × 2 m and the height was 1.5 m, and thus covered one-fourth of the model region. To compare with the single-point calculation results of the model applied with different methods, 25 receivers were set in the distance between the 45° diagonal direction of the grid and the centre of the power transformer group. Each receiver had a height of 1.5 m, and the horizontal coordinate interval of the different receivers was 2 m.

The distribution and geometric size of the point sources of the power transformer are shown in Fig. 9. In the analysis, the phase distribution characteristics of the sound source are considered, and the different transformers are uniformly divided into 35-point sources. The total sound power of each transformer is set as 100 dBA. Based on the actual field test result of the noise spectra, the dominant frequency of the power transformer is found to be 300 Hz, and thus the calculation frequency of the point source is chosen to be 300 Hz.

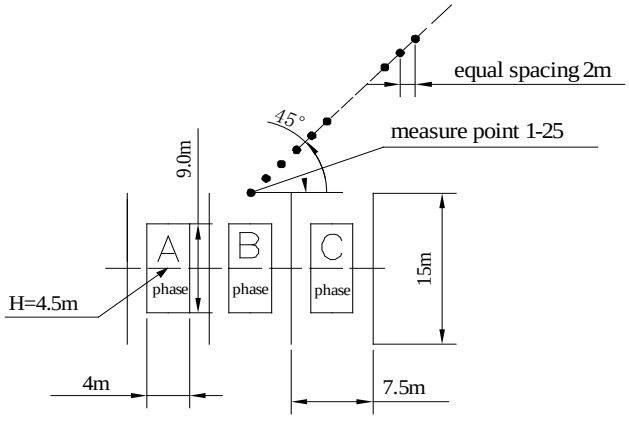


**Figure 9:** Noise source distribution and dimensions of the power transformer group

### *4.2 Results and Discussions*

Numerical simulations are performed by using the BEM, the Cadna/A prediction software based on ISO9613, and the proposed outdoor-coherent image source model. Fig. 10 plots the noise grid distribution of the power transformer group at 300 Hz calculated by the BEM for 160 hours. The noise map using the Cadna/A prediction software based on ISO9613, is shown in Fig. 11. The proposed coherent image source model of the power transformer group is calculated for 41 mins and the resultant noise grid distribution at 300 Hz is shown in Fig. 12.

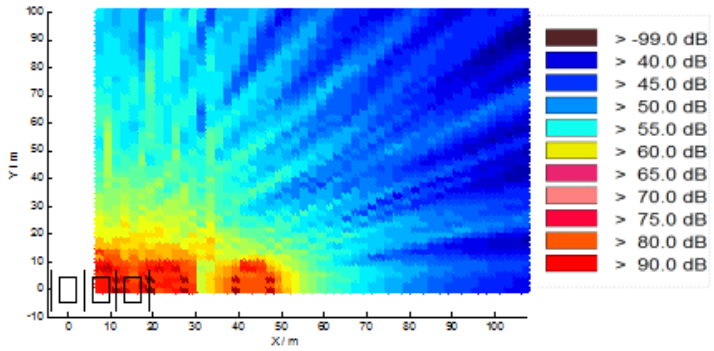


**Figure 10:** Noise distribution using the BEM

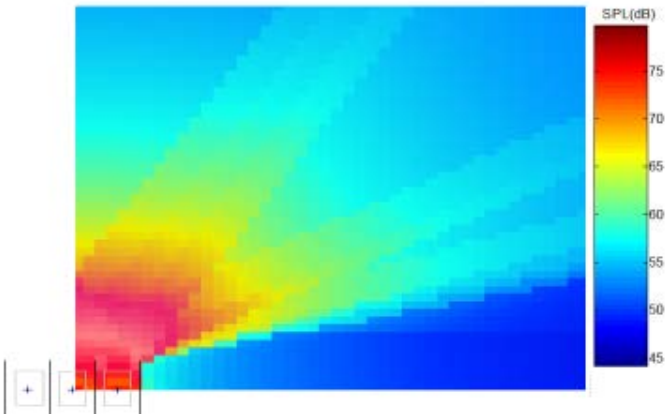


**Figure 11:** Noise distribution based on the ISO9613 model (Cadna/A)

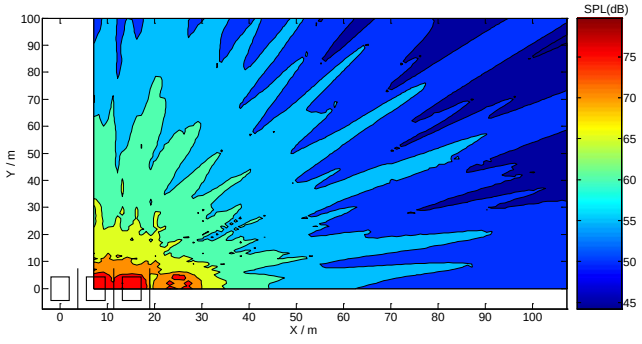


**Figure 12:** Noise distribution using the proposed calculation model

Comparing Figs. 10-12, it can be seen that the BEM and the proposed model are both capable of including the phases, and thus reflect the fluctuations of the coherent sound field. Interference fringes can

be clearly observed in the results by using these two methods. However, the Cadna/A prediction software based on ISO9613 does not lead to obvious interference fringes, since it only conducts energy superposition (without consideration of phase information). Furthermore, the noise maps obtained by the BEM and the proposed model as plotted in Figs. 10-12 respectively show similar colour and distribution trends. Comparison with the results shows good agreement between the BEM and the proposed model, with the latter having a significantly reduced computational cost.

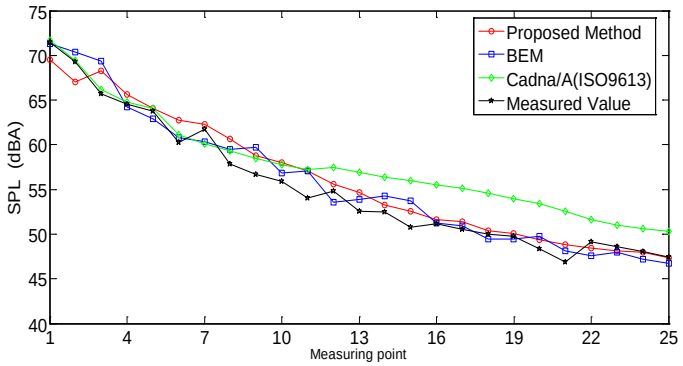


**Figure 13:** Predicted and measured SPLs at the receiver

Here, 25 receivers on the diagonal direction in the field grid are chosen for the calculation of the SPLs by the three aforementioned methods. Fig. 13 plots the calculated results in comparison with the measurement data. For the ISO9613 algorithm, it is found that the SPL decreases gradually when the distance between the receiver and the sound source increases. For the receiver close to the sound source, the SPL calculated using the ISO9613 algorithm is lower than those of the other two algorithms, since the superposition of the coherent image source is not included in the model. For the receiver far from the sound source, the SPL calculated by the ISO9613 algorithm is slightly higher. This is because the increase in the reflection loss caused by the changes of the sound ray and the incidence angle relative to the boundary surface with multiple reflections is neglected in the mirror image source method of the ISO9613 algorithm. Moreover, good agreement of the measurements and the predictions of the SPL by using the proposed method and the BEM. In general, the calculation error at the receivers is less than 2 dB, except at few receivers being 3 dB. In particular, for the receivers at the far field, the calculation error of the SPL is relatively small. This suggests that the proposed model is effective for reflecting the propagation trend of sound sources at different positions. Comparison results demonstrate that the proposed method offers a significant improvement over the BEM and the ISO9613 algorithm for outdoor noise predictions of power transformers.

## 5 Conclusions

This paper presents the outdoor-coherent image source model for the noise prediction induced by the power transformer. A scale model of the single-phase power transformer was first designed and tested. In the analysis, the power transformer is divided into several point sources, and the sound wave reflection coefficients of all boundaries generated by each image source and the receiver are subsequently calculated. The main advantage over the energy method lies in the fact that both the phase information and the spherical sound wave reflections at different boundaries are both included. The model has been used to predict the propagation noise from an actual power transformer group composed of three single-phase power transformers. Accurate prediction has been achieved by using the proposed model in comparison with the measurements. Moreover, it has been demonstrated that the proposed model outperforms the BEM and traditional ISO9613 algorithm for predicting noise propagation of the single-phase power transformers. This offers an improvement on the outdoor noise prediction accuracy of single-phase power transformers.

**Acknowledgements:** This work is funded by the Anhui Natural Science Foundation Project of China (under Grant KJ2016A201) and the National Natural Science Foundation of China (under Grant 11774378).

## References

1. Girgis, R. S., Bernesjö, M. S., Thomas, S., Anger, J., Chu, D. et al. (2011). Development of ultra-low-noise transformer technology. *IEEE Power and Energy Society General Meeting, 26*, 228-234.
2. AIEE Committee Report (1960). Bibliography on transformer noise. *IEEE Transactions on Power Apparatus and Systems, 79*, 735-740.
3. Wataru, K., Yoshiyuki, I., Toshiyuki, T., Akira, N. (2010). Analysis of structural deformation and vibration of a transformer core by using magnetic property of magnetostriction. *Electrical Engineering in Japan, 172*, 19-26.
4. Gordon, C. G. (1979). A method for prediction the audible noise emissions from large outdoors power transformers. *IEEE Transactions on Power Apparatus and Systems, 98*, 1109-1112.
5. Usry, G. O., Saha, P., Hadden, J. (1980). A method for prediction the audible noise emissions from large outdoors power transformers. *IEEE Transactions on Power Apparatus and Systems, 99*, 358-364.
6. Ming, R. S., Pan, J., Norton, M. P., Wende, S., Huang, H. (1999). The sound-field characterisation of a power transformer. *Applied Acoustics, 56*, 257-272.
7. Jin, M., Pan, J. (2016). Vibration transmission from internal structures to the tank of an oil-filled power transformer. *Applied Acoustics, 113*, 1-6.
8. Bai, B. D., Zhang, J., Yang, G. H., Wang, J. Y. (2012). Analysis of vibration and noise in transformer under DC Bias. *Applied Mechanics and Materials, 229-231*, 880-883.
9. Lin, C. E., Cheng, C. L., Huang, C. L., Yeh, J. C. (1993). Investigation of magnetizing inrush current in transformers. Part II - Harmonic analysis. *IEEE Transactions on Power Delivery, 8*, 255-263.
10. Beltle, M., Tenbohlen, S. (2012). Usability of vibration measurement for power transformer diagnosis and monitoring. *IEEE International Conference on Condition Monitoring and Diagnosis*, 281-284.
11. Muncey, R. W. (1950). The use of three-dimensional models in room acoustics. *Journal of the Acoustical Society of America, 22*, 510-511.
12. Min, H. Q., Qiu, X. J. (2009). Multiple acoustic diffraction around rigid parallel wide barriers. *Journal of the Acoustical Society of America, 126*, 179-186.
13. Lemire, G., Nicolas, J. (1989). Aerial propagation of spherical sound waves in bounded spaces. *Journal of the Acoustical Society of America, 85*, 1845-1853.
14. Attenborough, K., Hayek, S. I., Lawther, J. M. (1980). Propagation of sound above a porous half space. *Journal of the Acoustical Society of America, 68*, 1493-1501.
15. Kuttruff, H. (1991). *Room acoustic, 2nd ed*. London: Applied Science Publishers Limited.
16. Briquet, M., Filippi, P. (1977). Diffraction of a spherical wave by an absorbing plane. *Journal of the Acoustical Society of America, 61*, 640-646.
17. Embleton, T. F. W. (1996). Tutorial on sound propagation outdoors. *Journal of the Acoustical Society of America, 100*, 31-48.